A Fully Energy-Autonomous Temperature-to-Time Converter Powered by a Triboelectric Energy Harvester for Biomedical Applications

Joanne Si Ying Tan, *Student Member, IEEE*, Jeong Hoan Park, *Member, IEEE*, Jiamin Li, *Student Member, IEEE*, Yilong Dong, *Student Member, IEEE*, Kwok Hoe Chan, Ghim Wei Ho, and Jerald Yoo, *Senior Member, IEEE*

***Abstract*— This article presents a fully energy-autonomous temperature-to-time converter (TTC), entirely powered up by a triboelectric nanogenerator (TENG) for biomedical applications. Existing sensing systems either consume too much power to be sustained by energy harvesting or have poor accuracy. Also, the harvesting of low-frequency energy input has been challenging due to high reverse leakage of a rectifier. The proposed dynamic leakage suppression full-bridge rectifier (DLS-FBR) reduces the reverse leakage current by more than 1000×, enabling harvesting from sparse and sporadic energy sources; this enables the TTC to function with a TENG as the sole power source operating at <1-Hz human motion. Upon harvesting 0.6 V in the storage capacitor, the power management unit (PMU) activates the low-power TTC, which performs one-shot conversion of temperature to pulsewidth. Designed for biomedical applications, the TTC enables a temperature measurement range from 15 °C to 45 °C. The energy-autonomous TTC is fabricated in 0.18-μm 1P6M CMOS technology, consuming 0.14 pJ/conversion with 0.014-ms conversion time.**

***Index Terms*— Biomedical applications, dynamic leakage suppression full-bridge rectifier (DLS-FBR), energy harvesting, energy autonomous, Internet of Things (IoT), low leakage, low power, temperature-to-time converter (TTC).**

I. Introduction

TEMPERATURE information acquisition is essential in assessing and monitoring the operation conditions of sensor nodes/devices widely employed in assisted diagnostics, remote healthcare, and Internet-of-Things (IoT) nodes in general. With the devices worn or implanted in patients, overheating becomes detrimental to not only device performance but more importantly for tissues that suffer from thermal damage when exposed to high temperatures above 43 °C [1]. Therefore, implanted systems, such as [2] and [3], require temperature data to ensure patients' safety. Conversely, detection of temperatures below meaningful range detectable on body (<36 °C) could signal a potential detachment in need of prompt discovery and adjustment. Hence, the collection of temperature data is vital in biomedical devices for the safety of the patients and effectiveness of the monitoring devices.

Sensor nodes for biomedical IoT are numerous and widely distributed. For long-term monitoring, it is imperative to have sustainable and maintenance-free capabilities. One of the greatest limitations is the heavy reliance on batteries, an unsustainable source of power that requires replacement or cumbersome recharging [4]. Hence, it is essential for energy harvesting to supercede this depletable counterpart. Many energy harvester types are available, including pyroelectric, piezoelectric, triboelectric, and photovoltaic and radio frequency [5], [6]. For wearable or implanted devices, human motion is a readily available ambient source that is usually at frequencies below 1 Hz. Triboelectric nanogenerators (TENGs) are promising for harvesting such sparse human motion. However, although TENGs can produce large open-circuit voltages, the efficacy is severely restricted by the high reverse leakage current of full-bridge rectifiers (FBRs). As a result, storage of collected charges is impossible, especially at low harvesting frequencies of <1 Hz.

In addition, sensor nodes are required to function at extremely low voltages and power due to the efficiency limitations of energy harvesters. Recent temperature sensors [7]–[9], [12] consume microwatts of power. In addition, these sensors generally function at operating voltages (VDDLs) above 1 V, excessively high for energy-harvesting systems. Wang and Mercier [11] proposed a low-power temperature sensor; however, the inaccuracy is large even after two-point calibration.

To address these challenges and to achieve the energy-autonomous temperature sensing for IoT-based bio-applications, this article presents an ultra-low-power one-shot temperature-to-time converter (TTC) that operates at 0.6 V, with energy accumulation enabled by sporadic triboelectric

Manuscript received January 15, 2021; revised March 11, 2021 and April 30, 2021; accepted May 6, 2021. Date of publication May 26, 2021; date of current version September 24, 2021. This article was approved by Associate Editor Chen-Hao Chang. This work was supported in part by A*STAR AME Nanosystems at the Edge Program under Grant A18A4b0055 and in part by the Economic Development Board (EDB) Industrial Postgraduate Programme (IPP) of Singapore. *(Corresponding author: Jerald Yoo.)*

Joanne Si Ying Tan, Jiamin Li, Yilong Dong, Kwok Hoe Chan, and Ghim Wei Ho are with the Department of Electrical and Computer Engineering, National University of Singapore, Singapore 117583.

Jeong Hoan Park was with the Department of Electrical and Computer Engineering, National University of Singapore, Singapore 117583. He is now with Samsung Electronics, Hwaseong 18200, South Korea.

Jerald Yoo is with the Department of Electrical and Computer Engineering, National University of Singapore, Singapore 117583, and also with the N.1 Institute for Health, Singapore 117456 (e-mail: jyoo@nus.edu.sg).

Color versions of one or more figures in this article are available at https://doi.org/10.1109/JSSC.2021.3080383.

Digital Object Identifier 10.1109/JSSC.2021.3080383

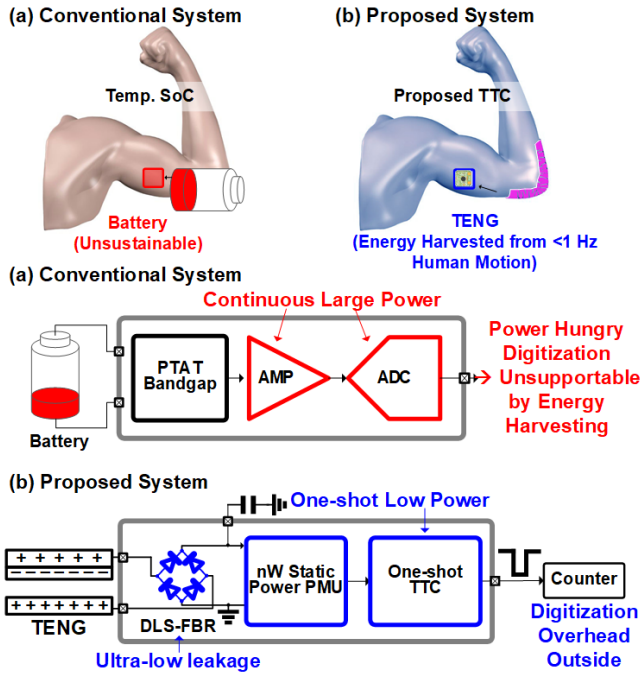

Fig. 1. System architecture of (a) conventional temperature sensing system and (b) proposed energy-autonomous system.

harvesting with the proposed dynamic leakage suppression full-bridge rectifier (DLS-FBR), shown in Fig. 1 [13]. The overall system achieves 0.14 pJ/conversion with only 5-nW stand-by power with the power management.

This article is organized as follows. Section II describes the overall architecture, TENG, and key design considerations of the proposed temperature sensing system. Section III delves into the circuit implementation and analysis. Section IV presents the measurement results. Section V discusses possible future work. Finally, Section VI concludes this article.

II. System Architecture and Triboelectric Harvester

A. Overall Architecture

Fig. 2 shows the overall architecture of the energy-autonomous TTC system. It consists of four main parts: the TENG, the >1000× leakage reduction DLS-FBR, nano-watt static power management unit (PMU), and ultra-low-power one-shot TTC. Fig. 3 shows the concept of the system. When the sparse input is given to the TENG, conventional FBR does not allow the accumulation of energy due to high reverse leakage. In contrast, the proposed DLS-FBR minimizes leakage dynamically, allowing the charge to accumulate. Upon sufficient energy accumulation, the PMU activates the one-shot TTC. Conventional temperature systems use amplifiers [7], [8] or oscillators [9], [10], [12] that are power-hungry. The proposed design uses a time-based charge accumulation scheme operating at a low supply of 0.6 V and outputs pulses encoding temperature information at only 0.14 pJ/conversion. The low voltage and power required, along with effective energy accumulation with DLS-FBR, allow the entire system to be sustained solely by the energy harvested from a TENG of <1-Hz frequency.

B. Triboelectric Energy Harvesting From Human Motion

To achieve energy-autonomous systems, the energy sources must be clean and sustainable. Fig. 4 compares the existing energy harvesters [4]. The efficiency of solar and RF is limited indoors and thermal harvesters rely on steep temperature gradients. Piezoelectric harvesters require high frequencies shown in Fig. 5. TENGs can scavenge ambient mechanical energy generated from human motion, with a frequency that can go down to 1 Hz. At such low frequencies, around microwatts of power per cm^2 could be expected. Furthermore, their flexible nature allows for future integration with wearable biosensors [17].

Fig. 6 shows the photograph of the TENG used in this article and its equivalent circuit model [18]. The harvester consists of a top conductive Ni-perfluoroalkoxy (PFA) layer and a bottom conductive Ni layer. Fig. 7 shows the measured characteristics of the harvester with 1-Hz actuation at contact separation mode for a 1 × 1 cm^2 active area. Fig. 7(a) shows the open-circuit output voltage, Fig. 7(b) shows the output voltage and current against load impedance, and Fig. 7(c) shows the power output against load impedance. Due to the dynamic nature of the DLS-FBR, load impedance (Z_{Load}) ranges from 5 MΩ at peak input voltage to hundreds of megaohms when the input pulse is rising or falling, shown in Fig. 7(b) and (c) as the Z-band of interest. The peak output power of the TENG lies within this Z_{Load} range, maximizing the harvested power. Voltage output reaches 4 V, while the current generated is low at <500 nA per pulse. Assuming that 1-Hz motion is maintained, the lowest power generated is around 500 nW, which is our power budget.

A major challenge for effective utilization of harvested energy is the high leakage in the system since the generated current is low. High reverse leakage current in conventional FBRs prevents harvested energy from being effectively sustained and accumulated, limiting its practicality. This is especially problematic in TENG for biomedical application, with the main source being the human motion that is generally of very low frequencies (<1 Hz). To solve this issue, we propose a DLS-FBR.

C. Ultra-Low-Power and Low Leakage Sensing

Power management is vital in energy-harvesting systems to provide a proper VDDL to the TTC. However, several challenges need to be addressed. The first is the slow ramping up of the harvested voltage (VDDLQ). The PMU must effectively supply only at the desired VDDL and cut off when the VDDLQ is insufficient for the accuracy of the TTC. The second is static power consumption. If the power consumption is too high, harvested energy will be wasted at the PMU and not reach the load.

Since the proposed TTC is designed for condition monitoring and assessing of devices worn on or implanted in patients, the sensing range should cover human body range with a

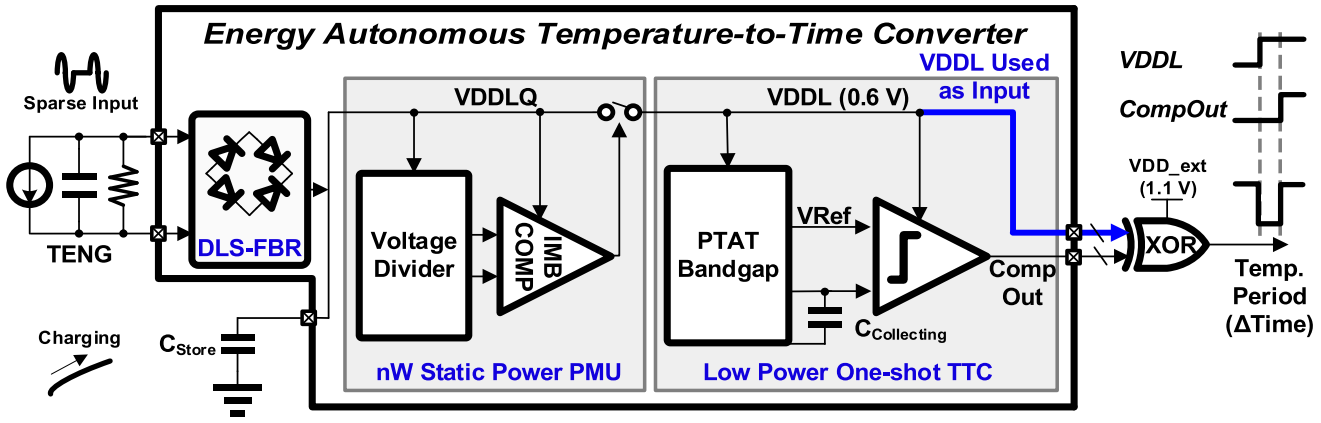

Fig. 2. Overall architecture of the proposed energy-autonomous TTC.

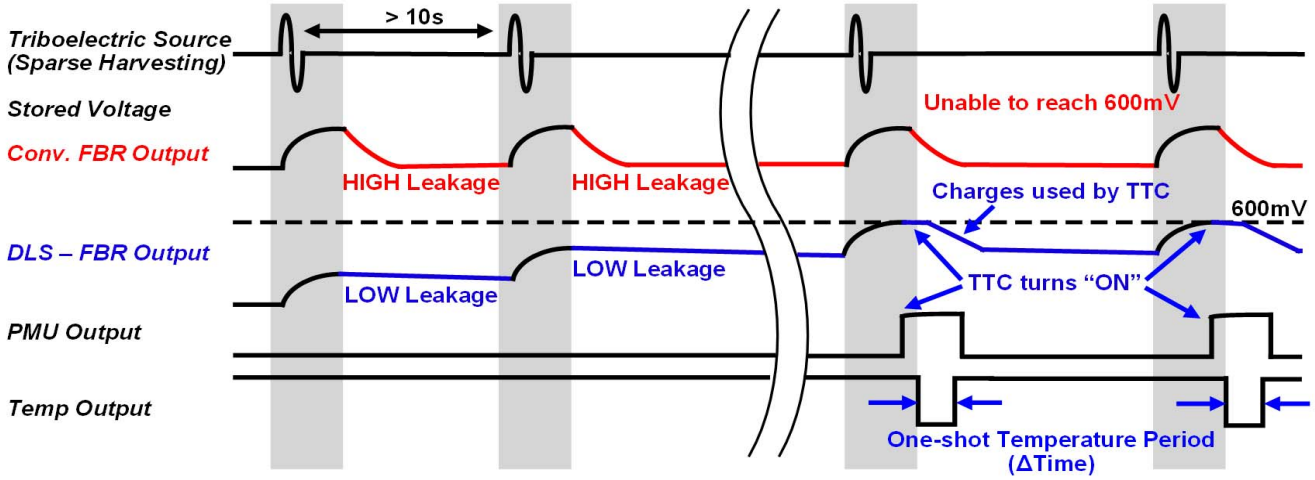

Fig. 3. Concept of the proposed energy-autonomous TTC.

Energy Source	Power Density	Frequency	Characteristics
Solar/PV	10μW/cm²(indoor) 15mW/cm²(outdoor)	DC	Requires exposure to light
RF Energy	0.1μW/cm²(GSM) 0.01μW/cm²(WiFi)	380M ~ 5 Hz	Low efficiency for indoor and out of line-of-sight
Thermal – body heat	40μW/cm²	DC	Requires high temperature differences
Piezoelectric	4μW/cm²	> 30 Hz	Not limited by indoors or outdoors
Triboelectric (TENG)	1μW/cm²	1 Hz	Not limited by indoors or outdoors

Fig. 4. Comparison of energy harvesters [4].

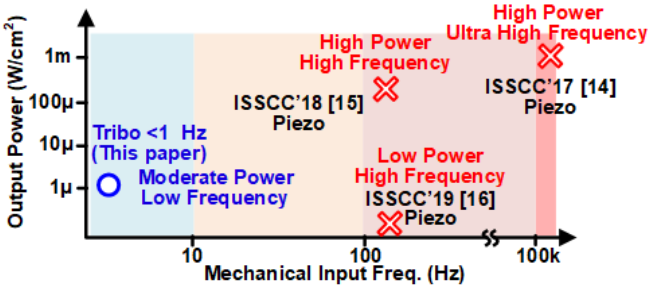

Fig. 5. TENG against other harvesters for low-frequency sources.

suitable margin for this application. The TTC is designed to target the range from 15 °C to 45 °C, more than sufficient for this application.

III. Building Blocks

To achieve ultra-low leakage and low-power sensing, our proposed energy-autonomous sensing system is explained in Sections III-A–III-C.

A. Dynamic Leakage Suppression Full-Bridge Rectifier

Figs. 8 and 9 show the leakage in conventional FBR and the leakage suppression of the novel DLS-FBR, respectively. At low frequency, leakage dominates the power dissipation, compared to the active power consumption. As depicted, idle transistors in conventional FBR suffer from high reverse leakage current. From our measurements with conventional FBRs, 79% of charge is leaked away within 1 s during a reverse-biased state when charged with a TENG operat-

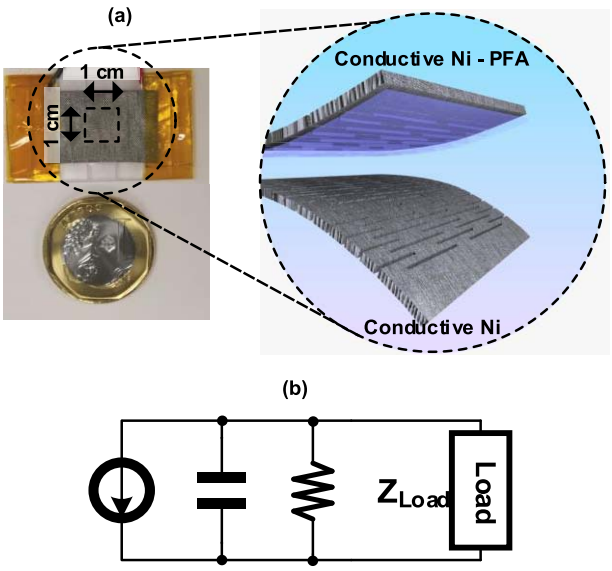

Fig. 6. (a) Photograph and (b) model of the TENG.

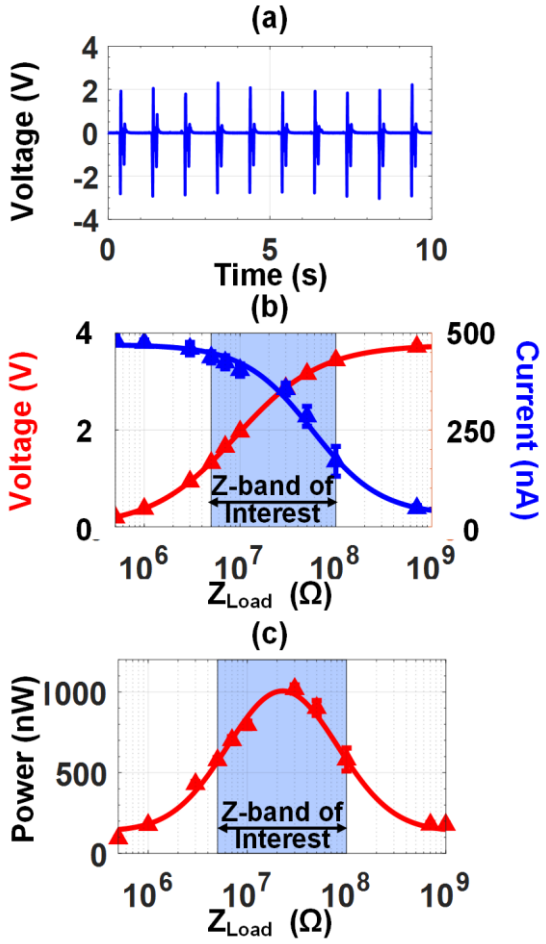

Fig. 7. Measurement results of (a) open-circuit output voltage of TENG (1×1 cm^2) shown in Fig. 6; (b) voltage and current relationship with load impedance; (c) peak power output against load impedance at actuation of 1 Hz.

ing at 1 Hz. Energy harvested from sparse voltage pulses below 1 Hz cannot be sufficiently accumulated if the rate of leakage is faster than accumulation. Hence, minimizing reverse leakage is vital. In the proposed design, four transistors, M5, M8, M9, and M12, are added, which suppresses leakage dynamically, dramatically enhancing the leakage reduction ability.

The proposed DLS-FBR trades off conversion efficiency to achieve leakage suppression, which dominates the harvested power dissipation, enabling voltage/energy accumulation for TTC activation. At the +Ve half input, where I_P is positive and I_N is negative, the current path formed by M5, M6, M11, and M12 charges the capacitor, while idle transistors M7–M10 are in super-cutoff state, reducing the OFF current along the potential leakage paths. When I_P becomes negative with the positive voltage at I_N, similar leakage suppression is illustrated. In contrast, transistors in OFF-state in conventional rectifiers, such as M2 and M3, will still exhibit leakage current between their drains and sources.

Fig. 10 analyzes the mechanism of the DLS. When the input is +Ve, current flows from I_P to O_P in Fig. 10(a). On the other hand, when the input is −Ve, current flows from I_P to O_N in Fig. 10(b). As shown in Fig. 10(a), when the positive voltage is at I_P, DLS is performed, with V_{GS} of NMOS and PMOS devices negatively self-biased in the super cutoff regions. Such V_{GS} values of the transistors are determined by the internal node, V_Y. Fig. 10(c) shows the relationship of the voltages in the input, output, and intermediate nodes. The idle transistors are in the super cutoff state as they have negative V_{GS}, and hence, ultra-low leakage is achieved. The internal node, V_X, determines V_{GS} of transistors in the top half that are turned on, forming a current path to charge the capacitor. When the negative voltage is at I_P, the regions flip, with the transistors at the top half in super cutoff and transistors at the bottom half forming a path for current flow.

Fig. 11 simulates the leakage in DLS-FBR across corners and temperature. Temperature and process variations can be seen to have a negligible effect on the leakage suppression ability of the DLS-FBR. In contrast to conventional architecture, DLS-FBR achieves an exceptional $>1000\times$ leakage reduction. Attributed to the DLS-FBR, self-sustaining the entire system by low-frequency TENG becomes possible.

B. Power Management Unit

Fig. 12 shows the schematic and functionality of the PMU. Due to the slow ramping up of the collected charges in VDDLQ, we require the PMU to enable the TTC only when the required voltage level of VDDL has been reached.

The imbalanced comparator (IMB COMP) monitors and detects the voltage difference between VB0 and VB1 that are obtained using a voltage divider of cascaded diode-connected PMOS transistors. To attain the ultra-low static current consumption of only 0.2 pA and low mismatch of the voltage divider PMOS chain, careful sizing and layout have been performed.

By sizing the two branches of the comparator with a ratio of 1:27, the PMU effectively turns on the TTC when the VDDLQ in the charge-collecting capacitor reaches the proper VDDL of 0.6 V.

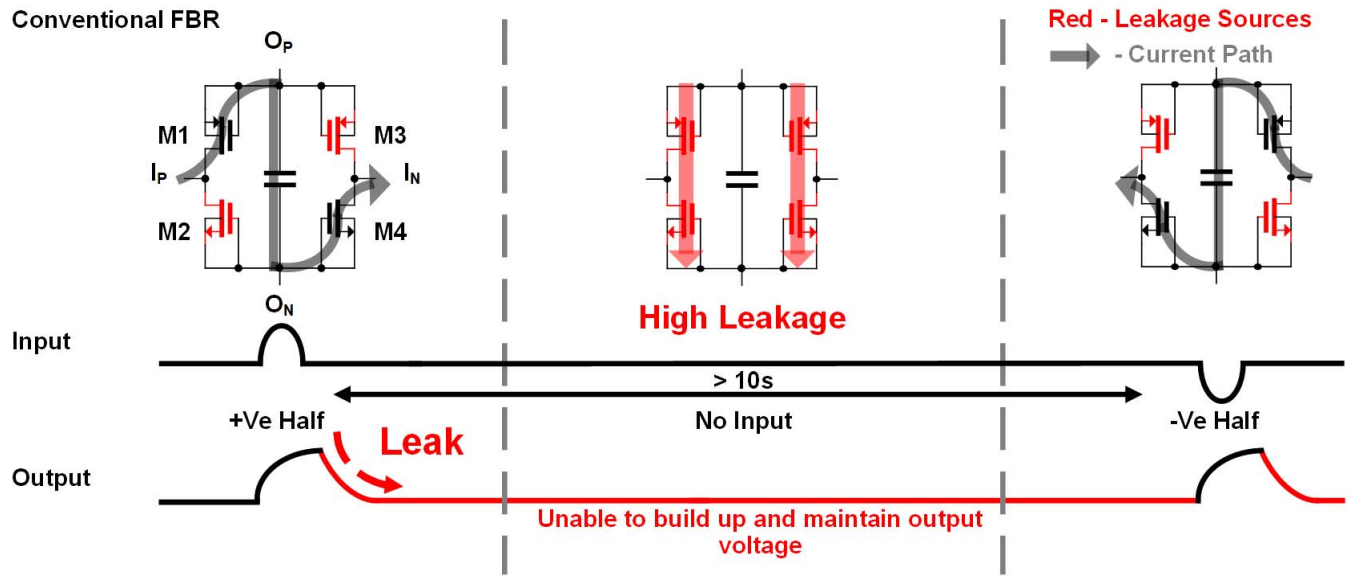

Fig. 8. Reverse leakage current sources in conventional FBR preventing voltage buildup.

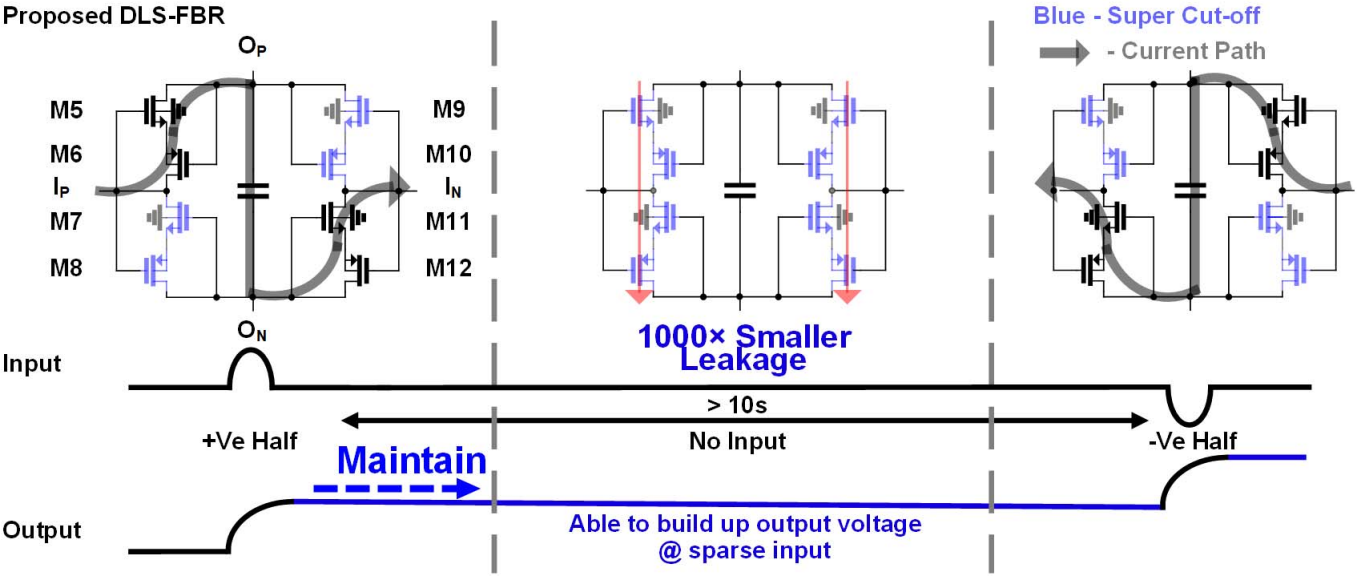

Fig. 9. Proposed DLS-FBR and the low leakage super cutoff regions allowing for voltage buildup.

From Fig. 7(b), we observe that the maximum output current is less than 500 nA. By selecting a 0.1 μF storage capacitor, each sparse input from TENG will contribute slightly to VDDLQ. From measurement results, we observe that each input pulse has a duration of <100 μs. Hence, the voltage contribution to VDDLQ by each triboelectric pulse can be calculated as follows:

$$V = \frac{Q}{C} = \frac{It}{C} = \frac{500 \times 10^{-9} \times 10^{-4}}{10^{-7}} = 500\ \mu\text{V}. \quad (1)$$

We observe that each triboelectric input pulse provides a 500-μV increase to the voltage collected that is supplied to the TTC. The instance collected voltage passes the threshold for TTC activation, PMU switches on the TTC and the charges are utilized to output the temperature pulse. When the voltage drops below the threshold after TTC activation, PMU shuts down the TTC and continues monitoring the VDDLQ level.

As a result, the system attains auto voltage regulation without requiring any regulator circuits that consume additional power. The PMU enables quick powering up and switching off of the TTC while consuming a meager 5 nW of static power during standby.

C. Low-Power TTC

The low-power TTC shown in Fig. 13 utilizes a bandgap reference that generates a current that is proportional to absolute temperature (IPTAT) to the charge-collecting capacitor, C1.

The bandgap reference consists of a current mirror, M14, M15, M19, and M20, which fixes the current ratio between

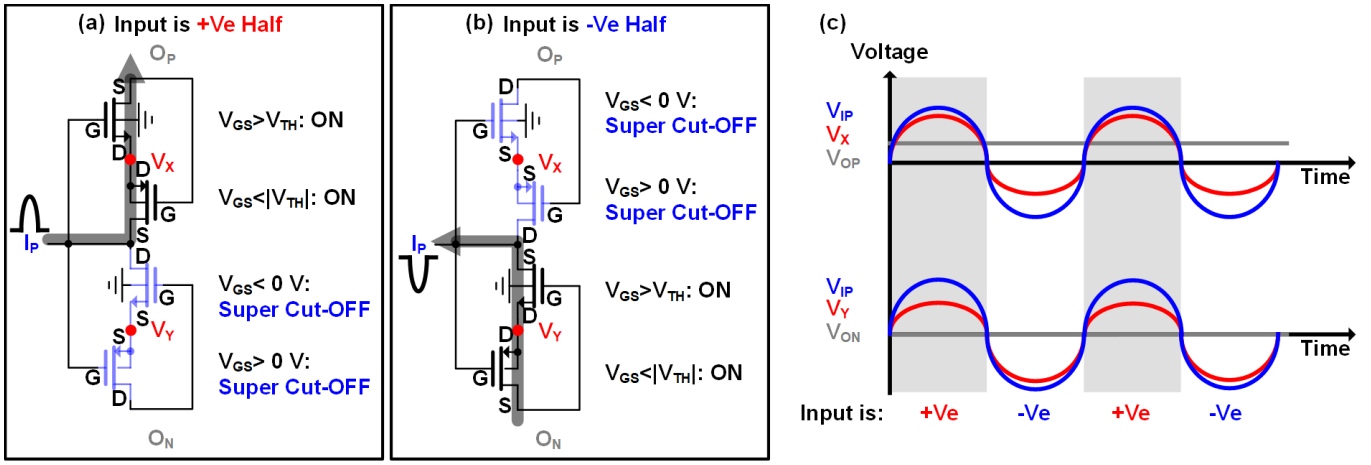

Fig. 10. Mechanism of DLS when (a) input is high, (b) input is low, and (c) relationship between voltages in the circuit.

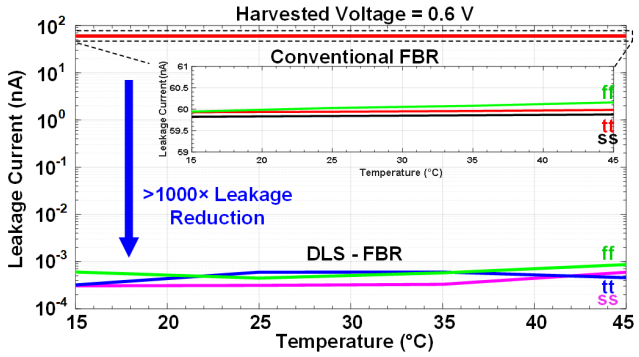

Fig. 11. Corner simulations of reverse leakage current against temperature.

the two branches; in our design, the ratio is 1:1 [19]. The Widlar current mirror, M16 and M21, defines the reference current, I, in the branch with M14, M15, M16, and M17. For our temperature sensing objective, we tuned the parameters of M16, M17, M21, and R1 in the bandgap reference for the particular temperature sensitivity desired.

Accumulated charge in C1 is compared against the voltage (VIN−) available inherently from the bandgap reference, thereby eliminating the need for an external reference that would otherwise consume additional power. Since our target is for human body temperature, the sensing range can be smaller (15 °C–45 °C). By adapting our design to the application, we are able to reduce the size of our charging capacitor, C1 (206.3 fF), for faster sensing as well as to dramatically reduce the power consumption of our TTC.

When the voltage across C1 is higher than the reference voltage, the comparator output, CompOut, toggles HIGH. Since IPTAT is dependent on temperature, C1 is charged at a rate proportional to temperature. To minimize power and circuitry, we utilize the period between the time the TTC turns on and the comparator giving an output, which is complementary to absolute temperature (CTAT), to obtain the temperature information. To visualize this CTAT period, VDDL and CompOut are compared using an on-chip XOR gate. Note that a separate 1 V (VDD_ext) is used as the supply

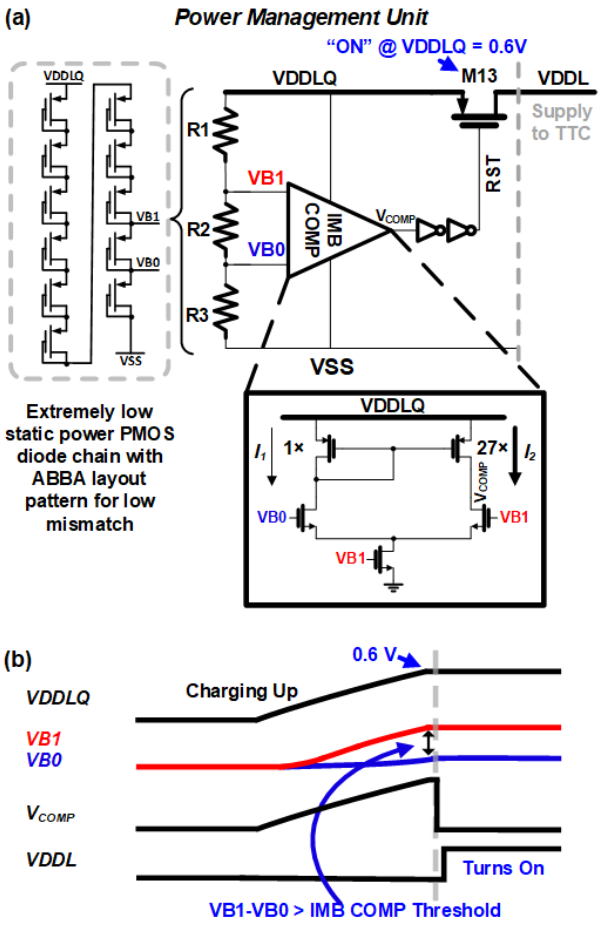

Fig. 12. (a) Schematic of PMU and IMB COMP and (b) functionality of the PMU.

for the XOR gate as the XOR gate is only used to display this CTAT period and not a part of the system. By using VDDL as the signal, we remove the need for a reference circuitry, thereby allowing for ultra-low-power operation. This pulse encoding the temperature reading (Δ time) is digitized externally to minimize power consumption and circuitry on

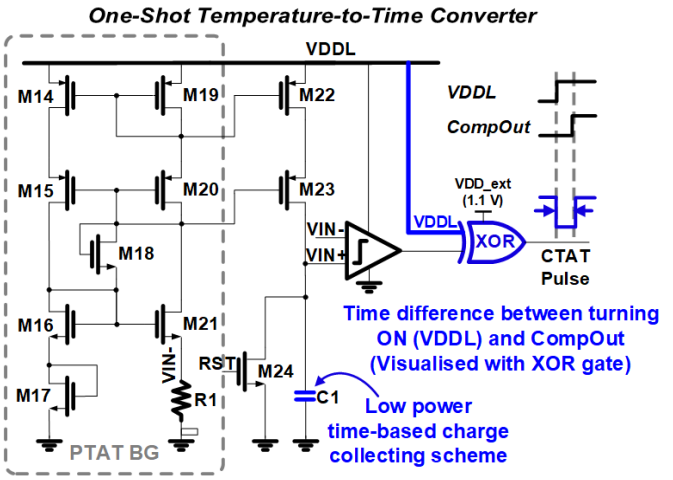

Fig. 13. Schematic of the low-power one-shot TTC with external XOR gate to visualize the time difference as a pulse.

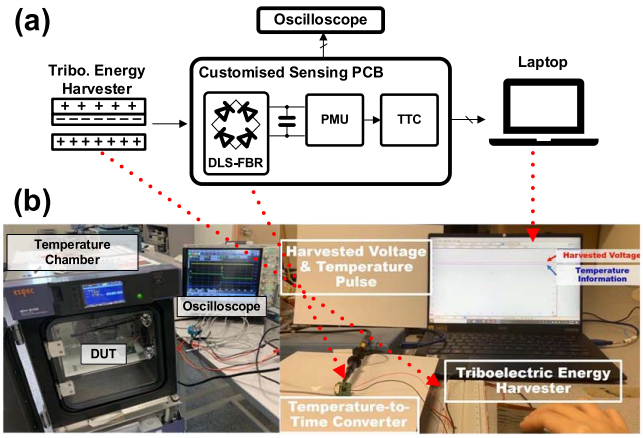

Fig. 14. (a) Block diagram of measurement setup and (b) photograph showing temperature chamber tests and processing of measured data on a laptop.

the human body. The scheme of time-based charge collection reads temperature with comparable sensitivity without power-hungry amplifiers or oscillators necessitated in conventional architectures. Combined with one-shot readout capability, the ultra-low-power TTC achieves 0.14 pJ/conversion.

IV. Measurement Results

Fig. 14 shows the measurement setup. A 1-Hz input is provided via hand tapping motion to the TENG. The ac harvester input is converted by the DLS-FBR and charges up the 0.1-μF storage capacitor. Measurements for the TTC are performed in the temperature chamber, sweeping the desired range from 15 °C to 45 °C. The temperature output is processed and calibrated via MATLAB.

A. Dynamic Leakage Suppression Full-Bridge Rectifier

Fig. 15(b) shows the measured stored voltage in the load capacitor when being charged by input pulses in 3-s intervals via the DLS-FBR. For comparison, a conventional FBR is fabricated and its measurements are presented in Fig. 15(a). Voltage is observed to fall significantly between successive

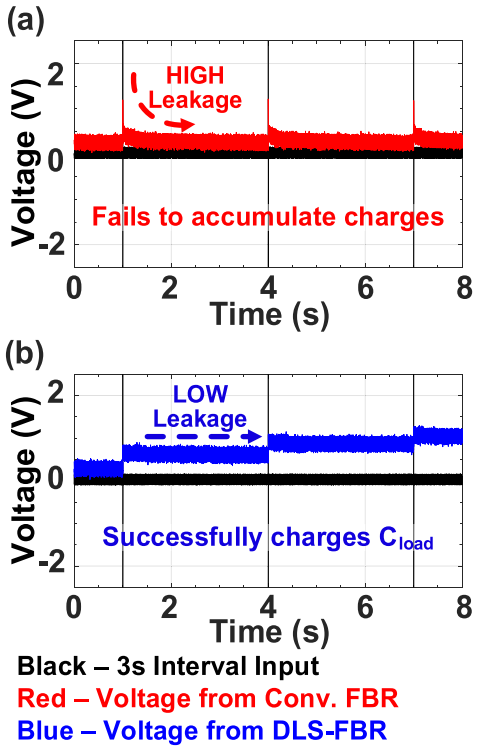

Fig. 15. Measurement results showing (a) leakage in conventional FBR versus (b) ability to sustain harvested energy with the proposed DLS-FBR.

input voltage pulses in the conventional FBR, indicating high leakage. In contrast, voltage is maintained for DLS-FBR, demonstrating that leakage is low.

Fig. 16 shows the variation of leakage in DLS-FBR with VDDLQ. Leakage in conventional FBR increases with VDDLQ, whereas it decreases in the DLS-FBR, showing a strong leakage suppression ability. From the measurement results, leakage of conventional FBR at 0.6-V VDDLQ is 7.41 μA, while the DLS-FBR achieves an exceptional $>1000\times$ leakage reduction to 27.5 pA.

We notice that the measured leakage is slightly higher than simulated results, which may be attributed to extra leakage from the pad and the storage capacitor; nevertheless, the collected voltage can be seen to maintain sufficiently for TTC activation.

B. Low-Power TTC

In Fig. 17(a), sparse harvesting from 1-Hz human motion charges up the collecting capacitor. When the VDDLQ reaches the TTC VDDL of 0.6 V, PMU will trigger the TTC to output VDDL and CompOut that has a CTAT time difference. To visualize the time difference, an XOR compares then and outputs a CTAT pulse. The pulsewidth (Δ time) determines the temperature, as shown in Fig. 17(b).

C. Decoding Temperature Information

The output temperature pulse is easily decoded via a simple counter at the receiver. We see the measured results of the TTC in Fig. 18. Process and temperature variations are reduced

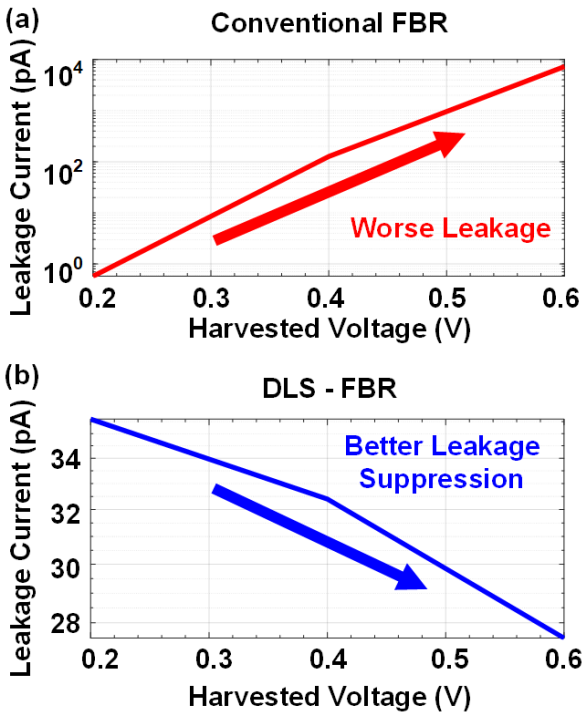

Harvested Voltage (V)	Leakage (nA)	
	Conv. FBR	DLS-FBR
0.2	0.72	0.0356
0.4	133	0.0324
0.6	7410	0.0275

Fig. 16. Measurement results of reverse leakage current against VDDLQ for (a) conventional FBR and (b) DLS-FBR.

via calibration. A one-point calibration is done for offset removal. The non-linearity is removed via a second-order curve fitting with lookup table. The accuracy achieved upon one-point calibration is sufficient for our application. The TTC measures the range from 15 °C to 45 °C and achieves ±1 °C inaccuracy upon one-point calibration, illustrating its pertinence in IoT-based biomedical monitoring. The counter is implemented on a field-programmable gate array (FPGA) with a counter frequency of 100 MHz to achieve 0.04 °C resolution. With calibration, the total power consumption of the counter is 163.4 μW, which can be supported by the much more generous power budget of the receiving station. By offloading the digitization overhead outside, we can achieve ultra-low-power energy-autonomous temperature detection nodes.

D. Power Consumption

During standby, the proposed system achieves a low-power consumption of 5 nW, as shown in Fig. 19. Fig. 20 shows the power breakdown of the system. The TTC and PMU consume 17.01 and 5.21 nW, respectively, when in operation. The low energy of 0.14 pJ/conversion allows for operation using only energy harvested from TENG at 1 Hz. Hence, energy-autonomous TTC is achieved.

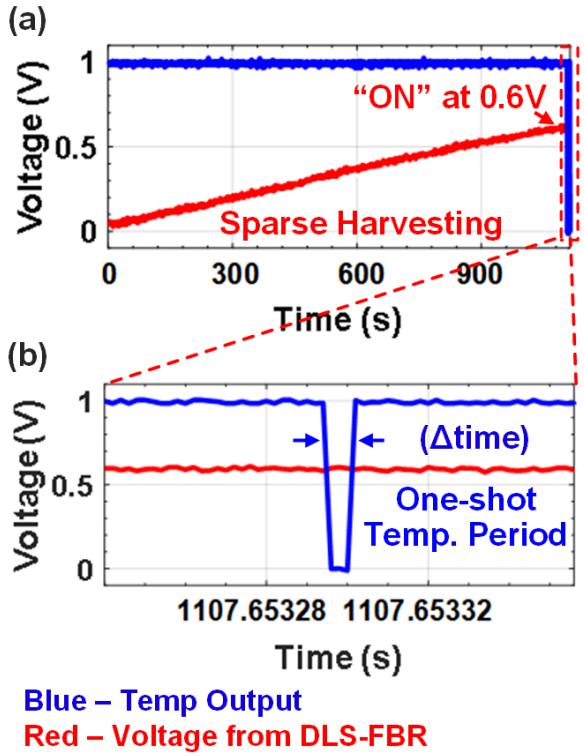

Fig. 17. Measurement results of (a) TTC activation upon sufficient harvested energy and (b) zoomed-in view of the temperature output pulse.

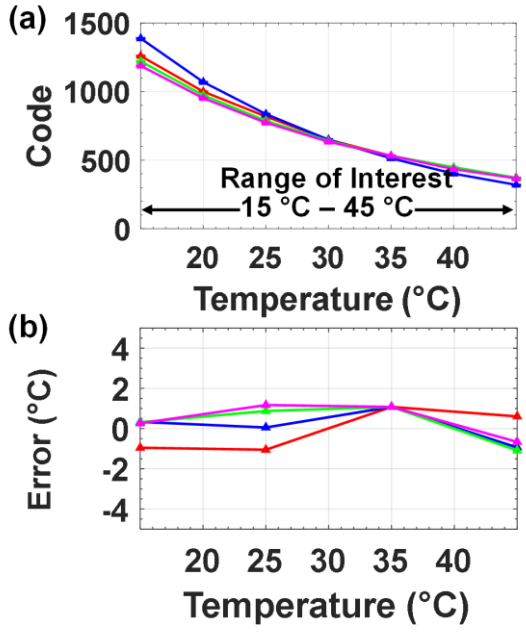

Fig. 18. Measurement results of (a) digital code against temperature after one-point calibration and (b) error graph.

E. Leakage Analysis

Fig. 21 compares the leakage breakdown in systems using conventional FBR and DLS-FBR during the energy accumulation period. Due to the high reverse leakage, the leakage of the conventional FBR dominates, causing the total system leakage to exceed the available capacity of 200 nA from the

TABLE I
PERFORMANCE COMPARISON WITH RECENT WORKS

Parameter	This Work	JSSC 2018 [7]	JSSC 2018 [8]	ISSCC 2018 [9]	JSSC 2019 [10]	JSSC 2019 [11]	JSSC 2020 [12]
Technology	**180 nm**	65 nm	180 nm	65 nm	180 nm	65 nm	55 nm
Energy Source	**TENG (< 1 Hz human motion)**	External Power Supply	External Power Supply	External Power Supply	External Power Supply	External Power Supply	External Power Supply
Type	**MOS**	Resistor	Resistor	Resistor	MOS	MOS	MOS
Conversion Type	**Temperature-to-Time**	Temperature-to-Digital	Temperature-to-Frequency	Temperature-to-Frequency	Temperature-to-Digital	Temperature-to-Digital	Temperature-to-Digital
Energy Autonomous	**Yes**	No	No	No	No	No	No
Energy/ Conversion (nJ)	**0.00014**	0.9	800	68	8.9	0.23	12.8
Power (μW)	**0.017**	12.8	160	68	0.011	0.0008	9.8
Supply (V)	**0.6**	1.1~1.4	1.8	0.85~1.05	0.8	0.5	0.8 ~ 1.3
Temp. Range (°C)	**15~45**	-40~110	-40~85	-40~85	-20~80	0~100	-40 ~ 125
Inaccuracy (°C)	**±1***	±1.05**	±0.2*	±0.35**	-0.9/+1.2**	-1.53/+1.61**	±0.94**
Conversion Time (ms)	**0.014**	0.08	5	1	839	300	1.31
Digitization Overhead Pushed Off-chip	**Yes**	No	Yes	Yes	No	No	No

*1-point **2-point

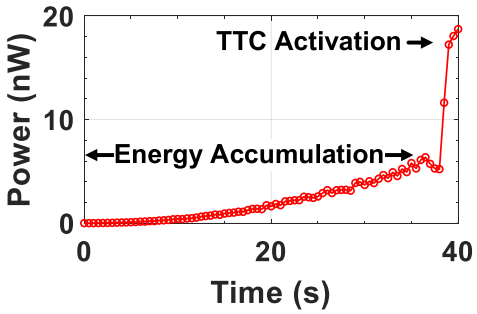

Fig. 19. Power consumption from "standby" to "ON" state of TTC with PMU.

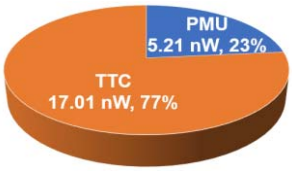

Fig. 20. Power breakdown.

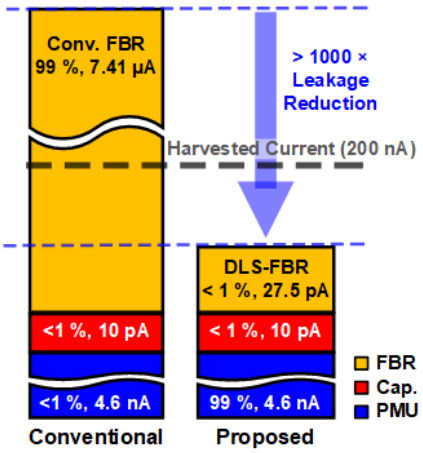

Fig. 21. Leakage breakdown in systems using conventional FBR versus proposed DLS-FBR during energy accumulation.

harvester. Hence, energy accumulation is not possible. On the other hand, the DLS-FBR effectively reduces this dominant leakage source by >1000×, pulling the total leakage below 200 nA, thereby achieving energy accumulation and enabling TTC activation.

V. DISCUSSION

Designed as a one-shot TTC, the proposed TTC operates at the low supply of 0.6 V, achieves the lowest energy/conversion, and has system power consumption of 5 nW at stand-by. With the DLS-FBR, reverse leakage current is reduced by more than 1000×, enabling the TTC to be solely powered by a TENG operated at <1-Hz human motion for the first time in the literature.

The converter is designed for expansion to a multi-channel system for simultaneous multi-node sensing in IoT systems. Because of the vast number of nodes, the capability of sending out the temperature information not only off-loads the energy burden on the sensing nodes, but also allows for multi-node monitoring at a centralized processing station.

Due to the stringent power budget for energy-autonomous systems, the communication method between the transmitter at

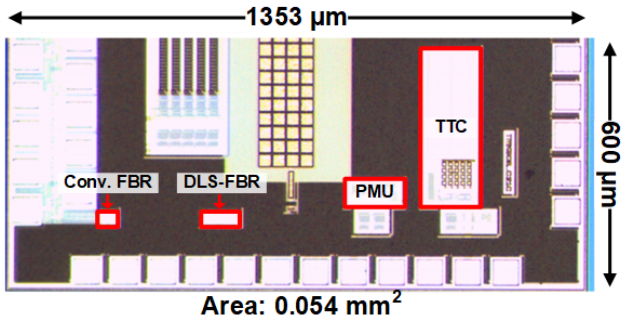

Fig. 22. Chip micrograph.

the node and receiver must be low in power. RF transmission has been enabled and reported to consume only 93.6 pW [20]. Hence, the sensing node with transmission of temperature data can be sustained via energy harvesting.

VI. Conclusion

This article presented an energy-autonomous TTC for biomedical applications. Table I presents the comparison with recent works. The chip micrograph, fabricated in 0.18-μm 1P6M CMOS, occupies an area of 0.054 mm^2 shown in Fig. 22.

Acknowledgment

The authors would like to thank Koh Chin Yeong and Philip Lim of Infineon Technologies Asia Pacific Pte. Ltd., Singapore, for their technical comments.

References

[1] P. S. Yarmolenko *et al.*, "Thresholds for thermal damage to normal tissues: An update," *Int. J. Hyperthermia*, vol. 27, no. 4, pp. 320–343, Jun. 2011.

[2] J. H. Park, J. S. Y. Tan, H. Wu, and J. Yoo, "34.2 1225-channel localized temperature-regulated neuromorphic retinal-prosthesis SoC with 56.3nW/channel image processor," in *IEEE Int. Solid-State Circuits Conf. (ISSCC) Dig. Tech. Papers*, vol. 63, Feb. 2020, pp. 508–510.

[3] J. H. Park, J. S. Y. Tan, H. Wu, Y. Dong, and J. Yoo, "1225-channel neuromorphic retinal-prosthesis SoC with localized temperature-regulation," *IEEE Trans. Biomed. Circuits Syst.*, vol. 14, no. 6, pp. 1232–1240, Dec. 2020.

[4] M. Shirvanimoghaddam *et al.*, "Towards a green and self-powered Internet of Things using piezoelectric energy harvesting," *IEEE Access*, vol. 7, pp. 94533–94556, 2019.

[5] J. Li *et al.*, "Human-body-coupled power-delivery and ambient-energy-harvesting ICs for a full-body-area power sustainability," in *IEEE Int. Solid-State Circuits Conf. (ISSCC) Dig. Tech. Papers*, vol. 63, Feb. 2020, pp. 514–515.

[6] J. Li, Y. Dong, J. H. Park, L. Lin, T. Tang, and J. Yoo, "Body-area powering with human body-coupled power transmission and energy harvesting ICs," *IEEE Trans. Biomed. Circuits Syst.*, vol. 14, no. 6, pp. 1263–1273, Dec. 2020.

[7] A. Mordakhay and J. Shor, "Miniaturized, 0.01 mm^2, resistor-based thermal sensor with an energy consumption of 0.9 nJ and a conversion time of 80 μs for processor applications," *IEEE J. Solid-State Circuits*, vol. 53, no. 10, pp. 2958–2969, Oct. 2018.

[8] S. Pan, Y. Luo, S. H. Shalmany, and K. A. A. Makinwa, "A resistor-based temperature sensor with a 0.13 pJ·K2 resolution FoM," *IEEE J. Solid-State Circuits*, vol. 53, no. 1, pp. 164–173, Jan. 2018.

[9] W. Choi *et al.*, "A 0.53 pJK^2 7000 μm^2 resistor-based temperature sensor with an inaccuracy of $\pm$0.35 °C (3σ) in 65 nm CMOS," in *IEEE Int. Solid-State Circuits Conf. (ISSCC) Dig. Tech. Papers*, vol. 61, Feb. 2018, pp. 322–324.

[10] T. Someya, A. K. M. M. Islam, T. Sakurai, and M. Takamiya, "An 11-nW CMOS temperature-to-digital converter utilizing sub-threshold current at sub-thermal drain voltage," *IEEE J. Solid-State Circuits*, vol. 54, no. 3, pp. 613–622, Mar. 2019.

[11] H. Wang and P. P. Mercier, "A 763 pW 230 pJ/Conversion fully integrated CMOS temperature-to-digital converter with +0.81 °C/−0.75 °C inaccuracy," *IEEE J. Solid-State Circuits*, vol. 54, no. 8, pp. 2281–2290, Aug. 2019.

[12] Z. Tang, Y. Fang, Z. Shi, X. Yu, N. N. Tan, and W. Pan, "A 1770-μm^2 leakage-based digital temperature sensor with supply sensitivity suppression in 55-nm CMOS," *IEEE J. Solid-State Circuits*, vol. 55, no. 3, pp. 781–793, Mar. 2020.

[13] J. S. Y. Tan *et al.*, "A 0.14 pJ/conversion fully energy-autonomous temperature-to-time converter for biomedical applications," *IEEE Solid-State Circuits Lett.*, vol. 3, pp. 466–469, 2020.

[14] Z. Chen, M.-K. Law, P.-I. Mak, W.-H. Ki, and R. P. Martins, "A 1.7 mm^2 inductorless fully integrated flipping-capacitor rectifier (FCR) for piezoelectric energy harvesting with 483% power-extraction enhancement," in *IEEE Int. Solid-State Circuits Conf. (ISSCC) Dig. Tech. Papers*, vol. 60, Feb. 2017, pp. 372–373.

[15] S. Du and A. A. Seshia, "A fully integrated split-electrode synchronized-switch-harvesting-on-capacitors (SE-SSHC) rectifier for piezoelectric energy harvesting with between 358% and 821% power-extraction enhancement," in *IEEE Int. Solid-State Circuits Conf. (ISSCC) Dig. Tech. Papers*, Feb. 2018, pp. 152–154.

[16] Z. Chen, Y. Jiang, M.-K. Law, P.-I. Mak, X. Zeng, and R. P. Martins, "A piezoelectric energy-harvesting interface using split-phase flipping-capacitor rectifier and capacitor reuse multiple-VCR SC DC-DC achieving 9.3× energy-extraction improvement," in *IEEE Int. Solid-State Circuits Conf. (ISSCC) Dig. Tech. Papers*, vol. 62, Feb. 2019, pp. 424–426.

[17] W. Paosangthong, R. Torah, and S. Beeby, "Recent progress on textile-based triboelectric nanogenerators," *Nano Energy*, vol. 55, pp. 401–423, Jan. 2019.

[18] I. Park, J. Maeng, D. Lim, M. Shim, J. Jeong, and C. Kim, "A 4.5-to-16 μW integrated triboelectric energy-harvesting system based on high-voltage dual-input buck converter with MPPT and 70 V maximum input voltage," in *IEEE Int. Solid-State Circuits Conf. (ISSCC) Dig. Tech. Papers*, vol. 61, Feb. 2018, pp. 146–148.

[19] F. Fiori and P. S. Crovetti, "A new compact temperature-compensated CMOS current reference," *IEEE Trans. Circuits Syst. II, Exp. Briefs*, vol. 52, no. 11, pp. 724–728, Nov. 2005.

[20] S. Bandyopadhyay, P. P. Mercier, A. C. Lysaght, K. M. Stankovic, and A. P. Chandrakasan, "A 1.1 nW energy-harvesting system with 544 pW quiescent power for next-generation implants," *IEEE J. Solid-State Circuits*, vol. 49, no. 12, pp. 2812–2824, Dec. 2014.

Joanne Si Ying Tan (Student Member, IEEE) received the B.Eng. and M.Eng. degrees in electrical engineering from the National University of Singapore (NUS), Singapore, in 2018 and 2020, respectively, where she is currently pursuing the Ph.D. degree with the Department of Electrical and Computer Engineering.

Her current research interest focuses on low-power temperature sensing systems.

Ms. Tan was a recipient/co-recipient of the IEEE International Solid-State Circuits Conference (ISSCC) 2020 Demonstration Session Certificate of Recognition (Demonstration Award) and ISSCC 2020 Student Travel Grant Award.

Jeong Hoan Park (Member, IEEE) received the B.S. and Ph.D. degrees from the School of Electrical Engineering and Computer Science, Seoul National University, Seoul, South Korea, in 2011 and 2017, respectively.

From 2017 to 2020, he has held a research fellow position at the Electrical and Computer Engineering Department, National University of Singapore, Singapore. He is currently a Staff Engineer with the DRAM Design Team, Samsung Electronics, Hwaseong, South Korea. His main research topics are developing low-power and low-noise multi-channel bio-signal acquisition and the neural prosthesis with neuromorphic processing system-on-chip (SoC). Also, he is interested in high-bandwidth memory (HBM).

Jiamin Li (Student Member, IEEE) received the B.Eng. degree in electrical engineering from the National University of Singapore (NUS), Singapore, in 2017, where she is currently pursuing the Ph.D. degree with the Department of Electrical and Computer Engineering.

Her research interests include the body-coupled powering for the body area network, power management, and mixed-signal integrated circuits and systems for wearable applications.

Ms. Li was a recipient/co-recipient of the 2020–2021 IEEE SSCS Predoctoral Achievement Award, ISSCC 2020 Demonstration Session Certificate of Recognition (Demonstration Award), and ISSCC 2020 Student Travel Grant Award.

Yilong Dong (Student Member, IEEE) received the B.Eng. degree in electrical engineering from the Dalian University of Technology (DUT), Dalian, China, in 2017. He is currently pursuing the Ph.D. degree with the Department of Electrical and Computer Engineering, National University of Singapore (NUS), Singapore.

His current research interests include body area power transfer circuits and systems for wireless wearable platforms.

Mr. Dong was a co-recipient of the ISSCC 2020 Demonstration Session Certificate of Recognition (Demonstration Award).

Kwok Hoe Chan received the B.Eng. (engineering science, specialization in nanoscience and nanotechnology) degree from the National University of Singapore, Singapore, in 2014.

He worked in developing nanogenerators for harvesting natural renewable energy sources.

Ghim Wei Ho received the B.Sc. and M.Sc. degrees from the National University of Singapore, Singapore, in 2000, and the Ph.D. degree from the University of Cambridge, Cambridge, U.K., in 2006.

Since 2006, she has been with the Department of Electrical and Computer Engineering, National University of Singapore, where she is currently a Full Professor and the Vice Dean of Student Life with the Faculty of Engineering. She leads the Sustainable Smart Solar System Research Group working on fundamental and applied research on nanosystems with emerging low dimensional nanomaterials, interfacial interactions, and hybridized functionalities for energy, environment, electronics, and healthcare. She has coauthored more than 150 articles in the international refereed journals.

Dr. Ho was an elected Scholar with the Selwyn College, University of Cambridge. She has been a Cambridge Commonwealth Society Fellow since 2006. In 2014, she was awarded the L'OREAL UNESCO for Women in Science Fellowship. In 2015, she was the honoree winner of the JCI's Ten Outstanding Young Persons (TOYP) Award in the science and/or technological development category. In 2016, she was honored as the Science and Technology Winner for the Great Women of Our Time as well as the ASEAN-US Science Prize for women. She is serving as an Associate Editor for *Journal of Materials Chemistry A* and *Materials Advances* and the Editorial Advisory Board of *Advanced Sustainable Systems*, *ChemPlusChem*, *Advanced Materials Technologies*, and *ChemNanoMat*.

Jerald Yoo (Senior Member, IEEE) received the B.S., M.S., and Ph.D. degrees from the Department of Electrical Engineering, Korea Advanced Institute of Science and Technology (KAIST), Daejeon, South Korea, in 2002, 2007, and 2010, respectively.

From 2010 to 2011, he was a Visiting Scholar with the Microsystems Technology Laboratories (MTL), Massachusetts Institute of Technology (MIT), Cambridge, MA, USA. From 2010 to 2016, he was with the Department of Electrical Engineering and Computer Science, Masdar Institute, Abu Dhabi, United Arab Emirates (UAE), where he was an Associate Professor. Since 2017, he has been with the Department of Electrical and Computer Engineering, National University of Singapore, Singapore, where he is currently an Associate Professor. He has pioneered research on body-area network (BAN) transceivers for communication/powering and wearable body sensor networks using the planar-fashionable circuit board for a continuous health monitoring system. He has authored book chapters in *Biomedical CMOS ICs* (Chapter 11, Springer, 2010), *Enabling the Internet of Things - From Circuits to Networks* (Chapter 12, Springer, 2017), and *The IoT Physical Layer* (Chapter 8, Springer, 2019). His current research interests include low-energy circuit technology for wearable bio-signal sensors, flexible circuit board platform, BAN for communication and powering, application-specified integrated circuit (ASIC) for piezoelectric micromachined ultrasonic transducers (pMUT), and system-on-chip (SoC) design to system realization for wearable healthcare applications.

Dr. Yoo is an IEEE Circuits and Systems Society (CASS) Distinguished Lecturer from 2019 to 2021. He also served as the IEEE Solid-State Circuits Society (SSCS) Distinguished Lecturer from 2017 to 2018. He was a recipient or a co-recipient of several awards: IEEE International Solid-State Circuits Conference (ISSCC) 2020 Demonstration Session Certificate of Recognition (Demonstration Award), IEEE International Symposium on Circuits and Systems (ISCAS) 2015 Best Paper Award (BioCAS Track), ISCAS 2015 Runner-Up Best Student Paper Award, the Masdar Institute Best Research Award in 2015, and the IEEE Asian Solid-State Circuits Conference (A-SSCC) Outstanding Design Award in 2005. He was the Founding Vice-Chair of IEEE SSCS UAE Chapter, and is currently the Chair of the IEEE SSCS Singapore Chapter. He currently serves as a Technical Program Committee Member of the IEEE ISSCC, ISSCC Student Research Preview (Co-Chair), IEEE Custom Integrated Circuits Conference (CICC, Emerging Technologies Subcommittee Chair), and IEEE A-SSCC (Emerging Technologies and Applications Subcommittee Chair). He is also an Analog Signal Processing Technical Committee Member of IEEE CASS. He has been an Associate Editor of IEEE OPEN JOURNAL OF THE SOLID-STATE CIRCUITS SOCIETY (OJ-SSCS) since 2021.